Journal of Hydrology 641 (2024) 131858

Contents lists available at ScienceDirect

Journal of Hydrology

journal homepage: www.elsevier.com/locate/jhydrol

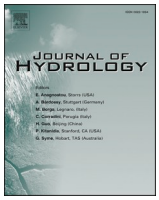

Research papers

Assessing a transitional and turbulent overland flow resistance law for surfaces with different roughness

Alessio Nicosia [a,*], Costanza Di Stefano [a], Vincenzo Palmeri [a,b], Maria Angela Serio [a], Vito Ferro [a,b]

[a] Department of Agricultural, Food and Forest Sciences, University of Palermo, Viale delle Scienze, Building 4, 90128 Palermo, Italy
[b] NBFC, National Biodiversity Future Center, 90133 Palermo, Italy

ARTICLE INFO

This manuscript was handled by Marco Borga, Editor-in-Chief, with the assistance of luca mao, Associate Editor

Keywords:
Overland flow
Roughness
Vegetation
Dimensional analysis
Self-similarity

ABSTRACT

The control and management of soil erosion phenomena caused by rainfall and runoff is a significant issue in sloping landscapes, especially if they are scarcely or not vegetated. The study of the relationship between soil roughness and flow resistance is a fundamental step in improving the knowledge of erosion processes. In this study, the suitability of a theoretically deduced flow resistance law, based on a power-velocity profile, was assessed by transitional and turbulent overland flow data obtained in laboratory and available in the literature. These measurements were obtained in a sloping (slope in the range 1–40 %) rectangular flume, testing the effects of six different roughness conditions. At first, for each investigated roughness condition, the available measurements were used to calibrate and test the equation relating the Γ function of the velocity distribution, the flow Froude number, and the channel slope. For all the investigated conditions, this analysis allowed for demonstrating that the flow resistance law gives a reliable estimate of the Darcy–Weisbach friction factor, with errors $\leq \pm 5$ % for 89.8–100 % of the examined cases with reference to the considered roughness condition. Then, using coefficients b (1.05) and c (0.562) of the Γ function available in the literature, the roughness effect was exclusively attributed to the a coefficient. In this case, the friction factor values calculated by the flow resistance law, with $b = 1.05$ and $c = 0.562$ and the a values corresponding to the different roughness conditions, are characterized by errors $\leq \pm 5\%$ for 70.4–100 % of the cases. Finally, the power relationships between the calibrated a, b, and c coefficients of the Γ function, and Manning's n values, corresponding to the roughness of the investigated surfaces, pointed out that the a coefficient is the most affected by the roughness conditions, as the exponent of Manning's assumes the highest value. The significance of this research is due to the fact that a relevant issue in modeling overland flow is to define the resistance coefficient for variable roughness, especially the vegetated ones.

1. Introduction

Controlling soil erosion phenomena caused by rainfall and runoff is one of the most significant challenges in the management of sloping hillslopes, particularly if there is no vegetation. Interrill and rill erosion are the principal processes occurring when sloping hillslopes are not appropriately shielded from rainfall and runoff. Erosion phenomena, roughness and hydrodynamic properties interact with each other. Overland flows can be recognized for their shallow water depths and limited bed shear stresses (Abrahams et al., 1994; Toy et al., 2002). According to Emmett (1970), the overland flow regime on hillslopes tend to vary from laminar at the hilltop to fully turbulent at some distance down the slope. Moreover, they have different flow regimes (i.e., from laminar to turbulent) (Cen et al., 2022) and hydraulic resistance characteristics in dependence of roughness characterizing the surface on which they move (i.e., bare soil, gravel, vegetated soil, etc.) (Ma et al., 2022; Liu et al., 2023; Zhang et al., 2024).

For smooth beds, some Authors (Yoon and Wenzel, 1971; Shen and Li, 1973) pointed out the influence of rainfall intensity on overland flow resistance for Reynolds number Re values less than 2000. For a rough bed made of glued sand grains, Katz et al. (1995) observed that flow resistance is influenced by raindrop impact and channel-bed roughness. Nearing et al. (2017) found an increasing relationship between slope and surface roughness, which counterbalances the expected increase in

* Corresponding author.
E-mail address: alessio.nicosia@unipa.it (A. Nicosia).

https://doi.org/10.1016/j.jhydrol.2024.131858
Received 24 November 2023; Received in revised form 26 July 2024; Accepted 8 August 2024
Available online 20 August 2024

flow velocity on steeper slopes. This condition, called "slope velocity equilibrium", is consequently due to the reciprocal influence between overland flow and soil surface morphology and is comparable with the feedback mechanism stated by Govers (1992) (Di Stefano et al., 2021; 2022a) for rill flows. Considering this hypothesis and the fact that slope and rainfall intensity affect the Darcy–Weisbach friction factor *f*, hydraulic equations like Manning and Darcy–Weisbach, are difficult to apply modeling runoff at hillslope scale.

Polyakov et al. (2018) reported the experiments performed at the Southwest Watershed Research Center for overland flows with rainfall simulation at the plot scale and with the presence of vegetation. These data were analyzed by Nicosia et al. (2020a), who presented a theoretical overland flow resistance law and found negligible effects of roughness on flow friction due to the laminar flow regime characterizing the experimental measurements.

Ferro and Nicosia (2020) tested a flow resistance law by the measurements reported in Sun et al. (2020) for tilled surfaces, characterized by different roughness conditions. The experimental measurements were used to determine the effect of the starting roughness and evaluate how the friction factor is affected by the temporal evolution of roughness. Their results highlighted that the starting roughness was influenced by the applied tillage method, and the flow resistance diminished during the experiment due to the flow modeling action. In fact, at the beginning of the experiments, both grain resistance and tillage-induced surface roughness constituted the total flow resistance, while, at the end of the experiments, the flow modeling action had reduced the surface roughness due to tillage and, consequently, its resistance.

Nicosia et al. (2020a; 2020b; 2020c) presented a theoretical overland flow resistance law, which is summarized below and in the Appendix A. The local flow velocity distribution $v(y)$ along a given vertical of an overland flow is represented by the following functional relationship (Barenblatt, 1987; 1993; Ferro, 1997):

$$\phi\left(\frac{dv}{dy}, y, h, d, u_*, s, i, \rho, \mu, g\right) = 0 \tag{1}$$

where ϕ is a functional symbol, y is the distance from the bottom, h is the water depth, d expresses the soil grain roughness, $u_* = (gRs)^{0.5}$ is the shear velocity, g is the gravitational acceleration, R is the hydraulic radius, s is the slope, i is the rainfall intensity, ρ is the water density, and μ is the water dynamic viscosity.

Applying the Π-theorem of the dimensional analysis (Barenblatt, 1987), Eq. (1) can be rewritten in the following dimensionless form:

$$\Pi_1 = \phi_1(\Pi_2, \Pi_3, \Pi_4, \Pi_5, \Pi_6, \Pi_7) \tag{2}$$

in which Π_1, Π_2, Π_3, Π_4, Π_5, Π_6 and Π_7 are dimensionless groups and ϕ_1 is a functional symbol.

The power velocity distribution (Eq. (10A), Appendix A) can be rearranged as:

$$\frac{v}{u_*} = \Gamma\left(\frac{u_* h}{\nu_k}, \frac{h}{d}, s, Re_i, F\right)\left(\frac{u_* y}{\nu_k}\right)^{\delta} \tag{3}$$

where $Re_i = i\,h/\nu_k$ is the rain Reynolds number (Nicosia et al., 2020c), ν_k is the kinematic viscosity, $F = V/(gh)^{0.5}$ is the Froude number, and δ can be obtained by the following relationship proposed by Castaing et al. (1990):

$$\delta = \frac{1.5}{\ln Re} \tag{4}$$

where $Re = V\,h/\nu_k$ is the Reynolds number.

As F accounts for the depth sediment ratio h/d and the shear Reynolds number $u_* h/\nu_k$ (Ferro, 2018), the velocity profile becomes:

$$\frac{v}{u_*} = \Gamma(s, Re_i, F)\left(\frac{u_* y}{\nu_k}\right)^{\delta} \tag{5}$$

By the integration of (Eq. (5)), the Darcy–Weisbach friction factor f is attained as (Di Stefano et al., 2017; Ferro, 2017; Ferro and Porto, 2018):

$$f = 8\left[\frac{2^{1-\delta}\Gamma Re^{\delta}}{(\delta+1)(\delta+2)}\right]^{-\frac{2}{1+\delta}} \tag{6}$$

Settling on $y = \alpha\, h$ (i.e., the distance from the bed where the local velocity equals the cross-section average velocity V) in Eq. (5), the expression Γ_v of the Γ function is the following (Ferro, 2017; Ferro and Porto, 2018):

$$\Gamma_v = \frac{V}{u_*\left(\frac{u_* \alpha h}{\nu_k}\right)^{\delta}} \tag{7}$$

where α (<1) is a coefficient which allows for not neglecting that V is located below the water surface and that the mean velocity profile is obtained by the mean, for each distance y, of the velocities v belonging to different verticals.

Ferro (2017) proposed the following theoretical equation to obtain α:

$$\alpha = \left[\frac{2^{1-\delta}}{(\delta+1)(\delta+2)}\right]^{1/\delta} \tag{8}$$

Several studies (Di Stefano et al., 2022b; Ferro, 2017; 2018; 2019; Nicosia et al., 2021), testing the applicability of Eq. (6) for different hydraulic conditions, applied the following relationships of Γ:

$$\Gamma_v = \frac{aF^b}{s^c} \tag{9}$$

$$\Gamma_v = \frac{aF^b}{s^c Re_i^{\,e}} \tag{10}$$

where a, b, c, and e are coefficients derived by the measurements. Obviously, Eq. (10) equals Eq. (9) for $e = 0$.

Nicosia et al. (2020b), utilizing experimental data reported in Nearing et al. (2017) for overland flows with rainfall simulations ($i = 59$ and 178 mm h^{-1}), established that Re cannot explain the rainfall effect and, consequently, both Re_i and Re are variables for predicting f. They demonstrated that Eq. (10) with $a = 0.323$, $b = 1.2833$, $c = 0.6698$, and $e = 0.0787$ leads to accurate Γ_v estimates, while Eq. (9) ($a = 0.4054$, $b = 1.2794$, $c = 0.6633$) gives underestimated and overestimated Γ_v values for $i = 59$ mm h^{-1} and overestimated for $i = 178$ mm h^{-1}, respectively.

The data reported in Polyakov et al. (2018) (4 vegetation types, s varying from 3.6 % to 39.6 %, $16 \le Re \le 709$, and $0.02 \le F \le 0.47$) were analyzed by Nicosia et al. (2020c), who proposed:

$$\Gamma_v = a\frac{F^{1.27}}{s^{0.68} Re_i^{0.056}} \tag{11}$$

where the a coefficient is dependent on the vegetation type. Even if the vegetation types were different, similar values of a coefficient were obtained, and this outcome was justified by the circumstance that the investigated flows were characterized by a laminar flow regime which determines negligible effects of roughness on flow resistance. Nevertheless, the results also highlighted that the best approach to estimate f is using a specific coefficient a for each vegetation type.

As suggested by Ferro and Nicosia (2020), the relationship between morphological surface roughness and hydraulic resistance can be a significant tool for fully understanding erosion phenomena and predicting some important variables, such as flow velocity. A significant issue in predicting overland flow is establishing the resistance coefficient for different surfaces (Kowobari et al., 1972). For this reason, in this study, a theoretical flow resistance law (Eq. (6)) (Ferro, 2017, 2018, 2019; Ferro and Porto, 2018) was used for the measurements by Hinsberger et al. (2022), performed for transitional and turbulent overland flows with different roughness conditions. The available data were used

for (i) testing the accuracy of the approach to estimate f; (ii) studying the effect of different roughness conditions on flow resistance; and (iii) establishing a relationship between the a, b, and c coefficients and Manning's n values, corresponding to the roughness of the investigated surfaces.

2. Database by Hinsberger et al. (2022)

In this investigation, the measurements performed by Hinsberger et al. (2022) were used (Hinsberger et al., (2021) [dataset] https://doi.org/10.6084/m9.figshare.17142440.v1). These measurements were carried out in a sloping (slope s varying from 1 to 40 %) rectangular flume, 0.5 m wide, 4 m long, and 0.35 m deep, with a coated plywood bottom and aluminum walls. During the experiments, the entire flume bed was covered with an inset. In particular, six different roughness conditions (aluminum, artificial grass, wheat, cement-based coating, asphaltic emulsion, and exposed aggregate concrete) were investigated. The flow discharge was measured by a magnetic-inductive flow meter, while water depth values were measured by a point gauge located in the flume axis to prevent disturbance due to the inlet and outlet areas. For the "wheat" runs, as the culms exceeded the flume walls, they were slightly bent at the top to measure the water depths. The two roughness conditions that investigate vegetation effects on flow behavior represent fully-submerged (artificial grass) and partially-submerged (wheat) vegetation.

A total of 730 data were collected. In Table 1, the ranges of slope, flow Froude number, and Reynolds number are listed. The investigated flows are always turbulent ($7061 \leq Re \leq 111258$) and both sub-critical and supercritical ($0.27 \leq F \leq 6.86$).

The available data were divided into six datasets, distinguished by the examined roughness condition. Then, each dataset was divided into two sub-datasets for calibrating and testing the theoretically-based flow resistance law. The division was made including measurements covering the whole experimental ranges for both the calibrating and testing sub-datasets.

3. Results

Fig. 1 clearly shows the trend of the Darcy–Weisbach friction factor values, $f=(8gRs)/V^2$, related to the roughness condition. In particular, as expected, the lowest values of f were obtained for aluminum, which is the smoothest examined surface, while the highest f values correspond to the two roughness conditions characterized by vegetation, i.e., wheat and artificial turf.

The available calibrating datasets were used to calibrate Eq. (9), and the obtained values of the a, b, and c coefficients are listed in Table 1. Fig. 2, as an example for the artificial turf condition, shows the comparison between the measured Γ_v values and those calculated by Eq. (9) with the a, b, and c coefficients listed in Table 1.

Substituting Eqs. (9) into Eq. (6), the following flow resistance equation was obtained:

$$f = 8\left[\frac{(\delta+1)(\delta+2)s^c}{2^{1-\delta}Re^{\delta}aF^b}\right]^{\frac{2}{1+\delta}} \tag{12}$$

in which δ is calculated by Eq. (4).

Fig. 3, as an example for the artificial turf condition, shows the good agreement between the measured f values and the ones calculated by Eq. (12) with the a, b, and c coefficients listed in Table 1. The friction factor values calculated by Eq. (12), introducing the corresponding values of the a, b, and c for each condition, are characterized by percentage of data falling into the error bands of ±5 % and ±2.5 % reported in Table 1.

Since the approach gave a good estimate of f for each roughness condition, the calibration was carried out for each whole dataset, obtaining the a, b, and c coefficients listed in Table 2. Fig. 4, as an example for the artificial turf condition, shows the comparison between the measured Γ_v values and those calculated by Eq. (9) with the a, b, and c coefficients listed in Table 2.

Fig. 5, as an example for the artificial turf condition, shows the good agreement between the measured friction factor values and the ones, f, calculated by Eq. (12) with the a, b, and c coefficients listed in Table 2. The Darcy–Weisbach friction factor values calculated by Eq. (12), introducing the corresponding values of a, b, and c for each condition, are characterized by the percentages of data falling into the error bands of ±5 % and ±2.5 % reported in Table 2.

Successively, the obtained mean values of b (1.05) and c (0.562) were fixed, and, investigating the behavior of the pairs (Γ, $X = F^{1.05}s^{-0.562}$) (Fig. 6), the a coefficient, equal to the slope coefficient of the best-fit straight line passing through the origin of the axes, corresponding to each roughness condition, was determined, obtaining the values listed in Table 3. Fig. 7 shows the comparison between the measured Γ_v values and those calculated by Eq. (9) with the a values listed in Table 3, and $b = 1.05$ and $c = 0.562$. Fig. 8 shows the agreement between the measured friction factor values and the ones, f, calculated by Eq. (12) introducing the corresponding a values listed in Table 3, and $b = 1.05$ and $c = 0.562$.

In this case, the friction factor values calculated by Eq. (12), and the corresponding a values listed in Table 3, and $b = 1.05$ and $c = 0.562$, are characterized by percentage of data falling into the error bands of ±5 % and ±2.5 % reported in Table 3.

Since the values of a listed in Table 3 are included in a small range, the mean value (0.3613) was used to test the applicability of a unique value independent of the roughness condition. Fig. 9 shows the comparison between the measured Γ_v values and those calculated by Eq. (9) with $a = 0.3613$, $b = 1.05$, and $c = 0.562$. Fig. 10 shows the agreement between the measured f and the ones calculated by Eq. (12) with $a =$

Table 1
Experimental ranges of s, Re, and F, and values of the a, b, and c coefficients of Eq. (9) estimated by the calibrating dataset, and percentage P_E of data falling into the error bands of ±5 % and ±2.5 %.

Roughness condition	Runs	s (%)	Re	F	a	b	c	P_E E ≤ ±5%	P_E E ≤ ±2.5 %
artificial turf	75(c) 74(t)	1–40	7375–111258	0.27–2.16	0.3307	1.1282	0.5883	100	98
wheat	39(c) 38(t)	1–35	7375–55551	0.42–2.28	0.3426	1.0704	0.5735	92.2	68.8
cement-based coating	84(c) 84(t)	1–40	7532–110317	1.32–4.97	0.3989	0.9992	0.5477	94	77.4
asphaltic emulsion	60(c) 59(t)	1–40	7061–110317	0.96–4.60	0.3906	1.0134	0.5476	98.3	90
exposed aggregate concrete	60(c) 59(t)	1–40	7061–110317	0.82–3.96	0.3698	1.0378	0.5565	100	99.1
aluminum	49(c) 49(t)	1–40	7846–110160	1.40–6.86	0.4402	0.9652	0.5328	90.8	45.9

c = calibrating; t = testing; P_E = percentage of cases in which errors in the estimate E are less than or equal to a given value (±5 and ± 2.5 %).

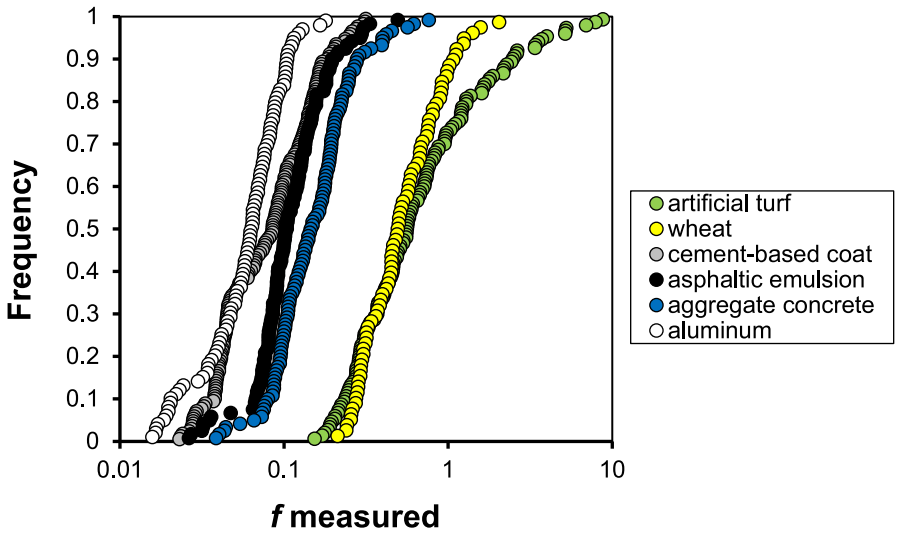

Fig. 1. Frequency distribution of the Darcy–Weisbach friction factor values related to the roughness condition.

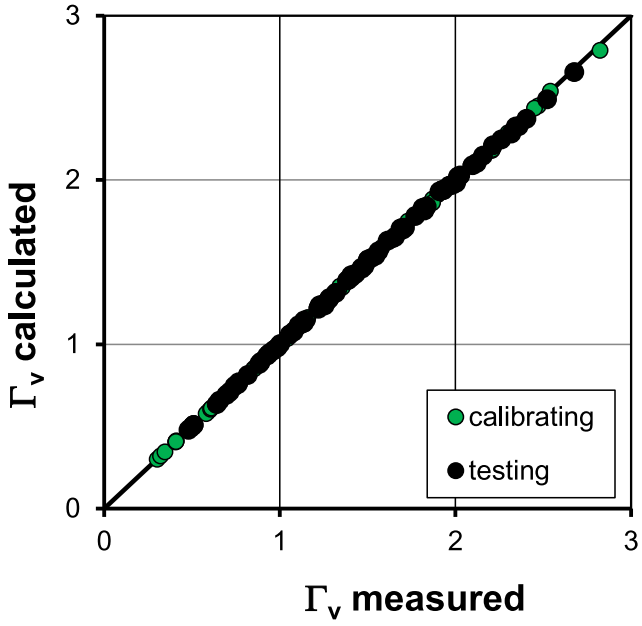

Fig. 2. Comparison, as an example for the artificial turf condition, between the measured Γ_v values and those calculated by Eq. (9) with the a, b, and c coefficients listed in Table 1.

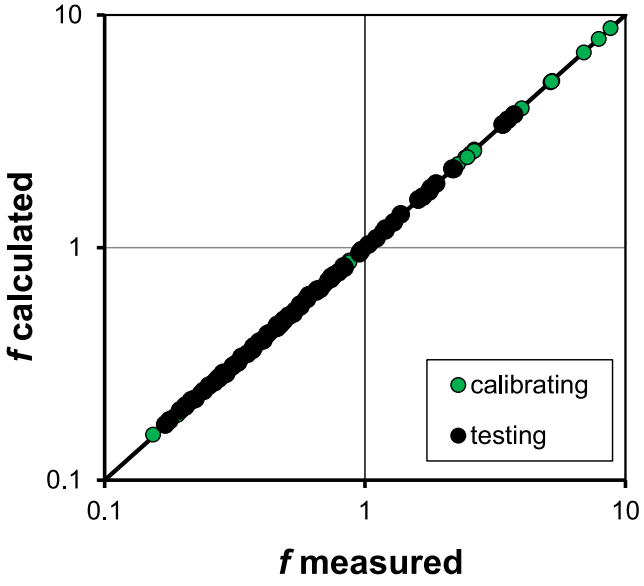

Fig. 3. Agreement, as an example for the artificial turf condition, between the measured friction factor values and the ones calculated by Eq. (12) with the a, b, and c coefficients listed in Table 1.

0.3613, $b = 1.05$, and $c = 0.562$. In this case, the friction factor values calculated by Eq. (12), with $a = 0.3613$, $b = 1.05$, and $c = 0.562$, are characterized by errors $\leq \pm 5\%$ for 81 % of cases and $\leq \pm 2.5$ % for 64.8 % of cases.

Notwithstanding the differences in terms of f highlighted by Fig. 1, the theoretical approach guarantees a reliable estimate of the Darcy–Weisbach friction factor also not considering the variability of the roughness condition, i.e., using the unique mean value of $a = 0.3613$ and fixing the b and c coefficients to 1.05 and 0.562, respectively. However, the best estimate of f is obtained when the roughness condition is considered calibrating Eq. (9) for the whole dataset for each roughness condition.

At last, the values of the a, b, and c coefficients (Table 2) were related with the mean Manning's n values, calculated as $n = (s^{1/2}\ R^{2/3})/V$, corresponding to the examined surfaces and their roughness (Fig. 11). Fig. 11 points out that the estimated coefficients are strictly related with

Table 2
Values of a, b, and c coefficients obtained calibrating Eq. (9) for each whole dataset, and percentage of data falling into the error bands of ±5 % and ±2.5 %.

	runs	a	b	c	P_E E ≤ ±5%	P_E E ≤ ±2.5 %
artificial turf	149	0.3305	1.1286	−0.5888	100	98.6
wheat	77	0.3408	1.0781	−0.5757	90.9	70.1
cement-based coating	168	0.3802	1.0277	−0.5550	95.8	82.1
asphaltic emulsion	119	0.3863	1.0199	−0.5494	99.1	89.9
exposed aggregate concrete	119	0.3665	1.0438	−0.5582	100	97.5
aluminum	98	0.4067	1.0045	−0.5446	89.8	60.2

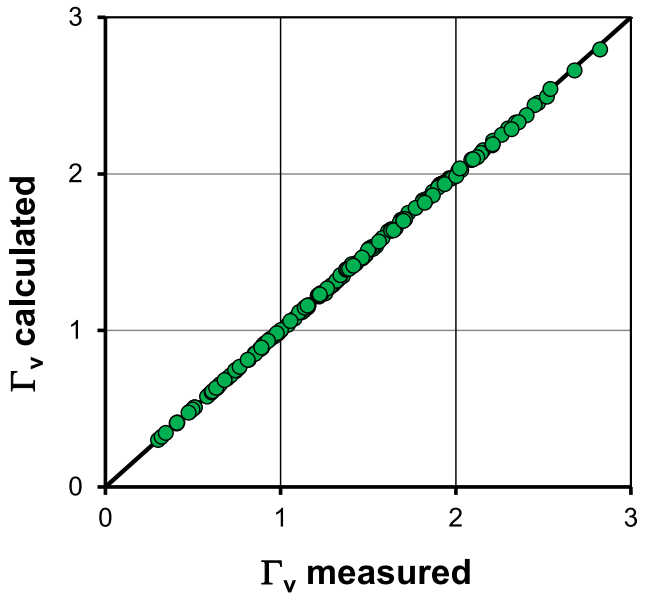

Fig. 4. Comparison, as an example for the artificial turf condition, between the measured Γ_v values and those calculated by Eq. (9) with the a, b, and c coefficients listed in Table 2.

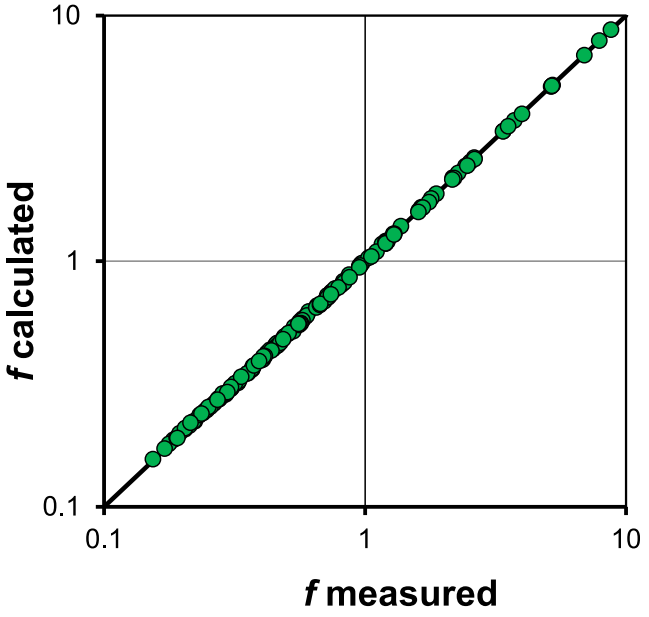

Fig. 5. Comparison, as an example for the artificial turf condition, between the measured friction factor values and the ones calculated by Eq. (12) with the a, b, and c coefficients listed in Table 2.

the Manning's n according to the following relationships:

$$a = 0.2245n^{-0.137} \quad (13)$$

$$b = 1.3694n^{0.0741} \quad (14)$$

$$c = 0.6771n^{0.052} \quad (15)$$

4. Discussion

For the artificial turf condition, as an example, Fig. 2 shows that Eq. (9), whose a, b, and c coefficients were estimated by the calibrating subdataset (Table 1), is positively tested by the independent testing subdataset and the obtained flow resistance law (Eq. (12)) allows a reliable estimate of the Darcy–Weisbach friction factor. The agreement between the measured f values and those calculated by Eq. (12) is characterized by errors in the estimate (Table 1) that, for 91–100 % of the cases, are $\leq \pm$ 5 %.

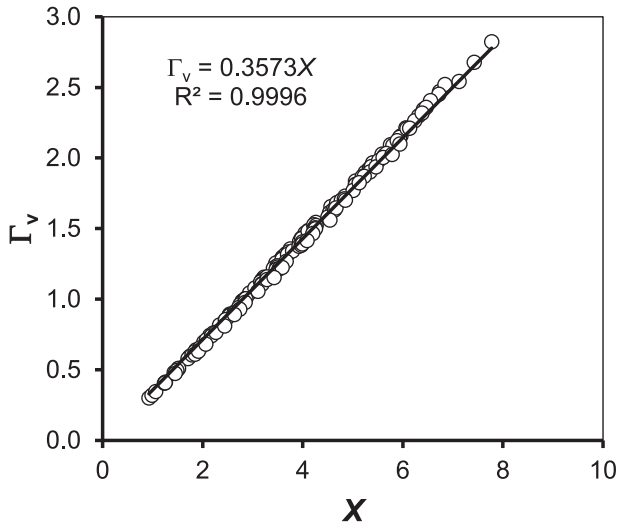

Fig. 6. Pairs (Γ, $X = F^{1.05}\, s^{-0.562}$) for the artificial turf condition.

Table 3
Values of the a coefficients obtained fixing $b = 1.05$ and $c = 0.562$, and percentage of data falling into the error bands of ±5 % and ±2.5 %.

	a with $b = 1.05$ and $c = 0.562$	P_E E ≤ ±5%	P_E E ≤ ±2.5 %
artificial turf	0.3573	70.6	43.0
wheat	0.3544	92.2	54.5
cement-based coating	0.3646	92.2	86.3
asphaltic emulsion	0.3632	95.8	88.2
exposed aggregate concrete	0.3611	100	96.6
aluminum	0.3672	87.7	74.5
Mean	0.3613	89.7	73.86

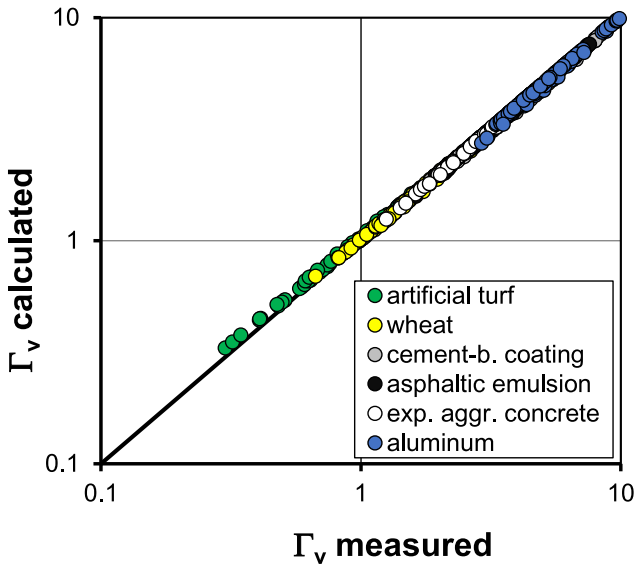

Fig. 7. Comparison between the measured Γ_v values and those calculated by Eq. (9) with a values listed in Table 3, and $b = 1.05$ and $c = 0.562$.

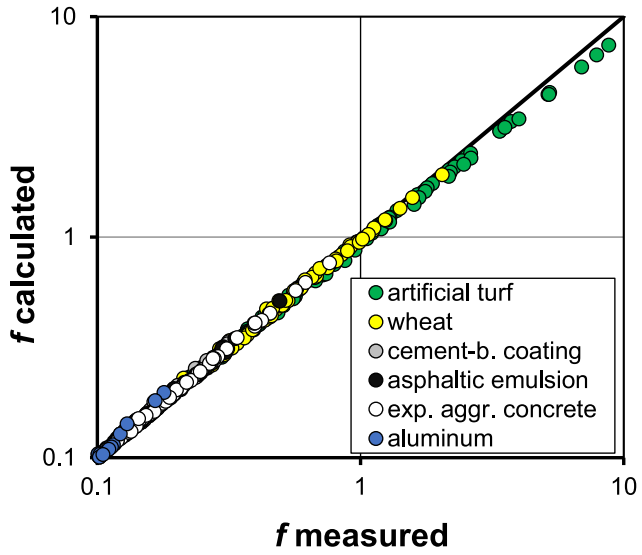

Fig. 8. Comparison between the measured friction factor values and the ones calculated by Eq. (12) introducing the corresponding a values listed in Table 3, and $b = 1.05$ and $c = 0.562$.

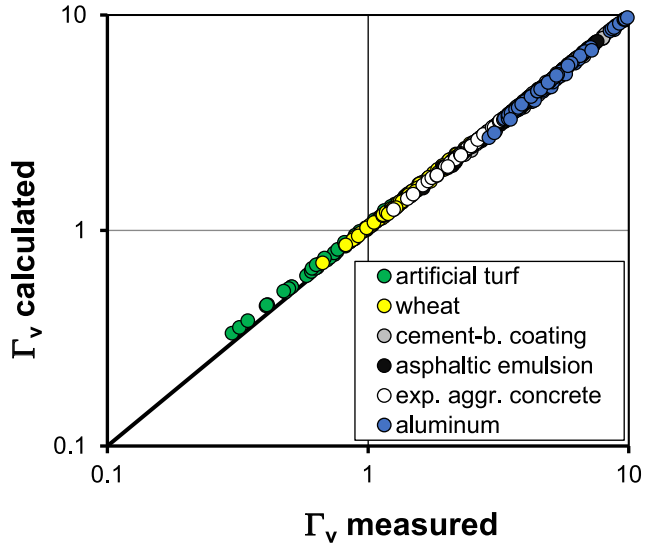

Fig. 9. Comparison between the measured Γ_v values and those calculated by Eq. (9) with $a = 0.3613$, $b = 1.05$, and $c = 0.562$.

For the artificial turf condition, if the whole database is considered for estimating the a, b, and c coefficients (Table 2), the agreement between the measured f values and those calculated by Eq. (12) is characterized by estimate errors (Table 2) that for 89.8–100 % of the cases are $\leq \pm$ 5 %. The percentage of data falling into the error bands of ±5 % (Table 2) is not related to the investigated roughness condition, confirming that the theoretical flow resistance equation is able to give an accurate estimate of the Darcy–Weisbach friction factor for different roughness and hydraulic conditions (Di Stefano et al., 2022b; Ferro, 2017; 2018; 2019; Nicosia et al., 2021).

Considering, as obtained in previous investigations (Nicosia and Ferro, 2023), that the exponents b (1.05) of the Froude number and c (0.562) of slope can be assumed independent of the investigated roughness condition, the effect of roughness was explained exclusively by the a coefficient (Table 3). The good agreement (Fig. 8) between the measured friction factor values and the ones, f, calculated by Eq. (12), with $b = 1.05$, $c = 0.562$ and the corresponding a values listed in Table 3,

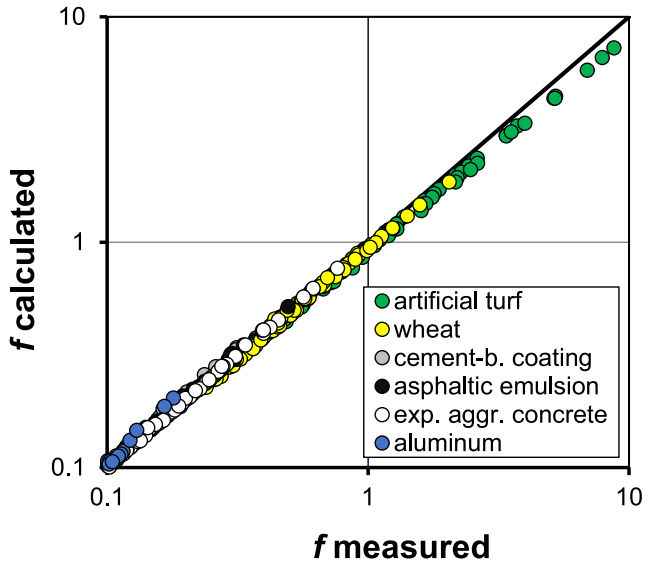

Fig. 10. Comparison between the measured friction factor values and the ones calculated by Eq. (12) with $a = 0.3613$, $b = 1.05$, and $c = 0.562$.

confirms the reliability of the hypothesis to use a as the single coefficient affected by the roughness condition. The agreement between the measured f values and those calculated by Eq. (12), with $b = 1.05$, $c = 0.562$ and the corresponding a values listed in Table 3, is characterized by estimate errors (Table 3) that for 70.4–100 % of the cases are less than or equal to ±5 %.

Since the values of a listed in Table 3 are included in a narrow range, the hypothesis to use an average value of a coefficient (0.3613) independent of the roughness condition was also tested. This theoretical approach (Eq. (12)) with $a = 0.3613$, $b = 1.05$, and $c = 0.562$) guarantees a good estimate of the Darcy–Weisbach friction factor even if the flow resistance tends to be underestimated for the vegetated conditions (wheat, artificial turf) (Fig. 10).

The relationships between the a, b, and c coefficients (Table 2) and Manning's n values, corresponding to the investigated surfaces and their roughness, (Fig. 11) pointed out that a different effect of the Manning's n on the considered coefficient can be observed. In particular, the comparison among Eqs. (13), (14), and (15) highlighted that a is the most affected by roughness conditions as the exponent of Manning's assumes the highest value.

In conclusion, the applied theoretical approach can give an accurate estimate of the Darcy–Weisbach friction factor and account for the surface roughness. The obtained results can help in modeling overland flow defining the resistance coefficient for variable roughness, especially the vegetated ones.

5. Conclusions

Laboratory measurements, performed by Hinsberger et al. (2022) in a flume characterized by six roughness conditions (aluminum, artificial grass, wheat, cement-based coating, asphaltic emulsion, and exposed aggregate concrete), were utilized to verify the reliability of a theoretical flow resistance equation suggested by Ferro (2019) and already calibrated for vegetated channels and gravel-bed rivers. This equation was calibrated by the analysis of the relationship between Γ, F, and s of the six data sets. Considering, as obtained in previous investigations, that the exponents b (1.05) of the Froude number and c (0.562) of slope can be assumed independent of the investigated roughness condition, the hypothesis of explaining the effect of roughness exclusively by the a coefficient was also tested. The good agreement between the measured friction factor values and the ones calculated by Eq. (12), with $b = 1.05$, $c = 0.562$ and the corresponding a values listed in Table 3, confirmed the

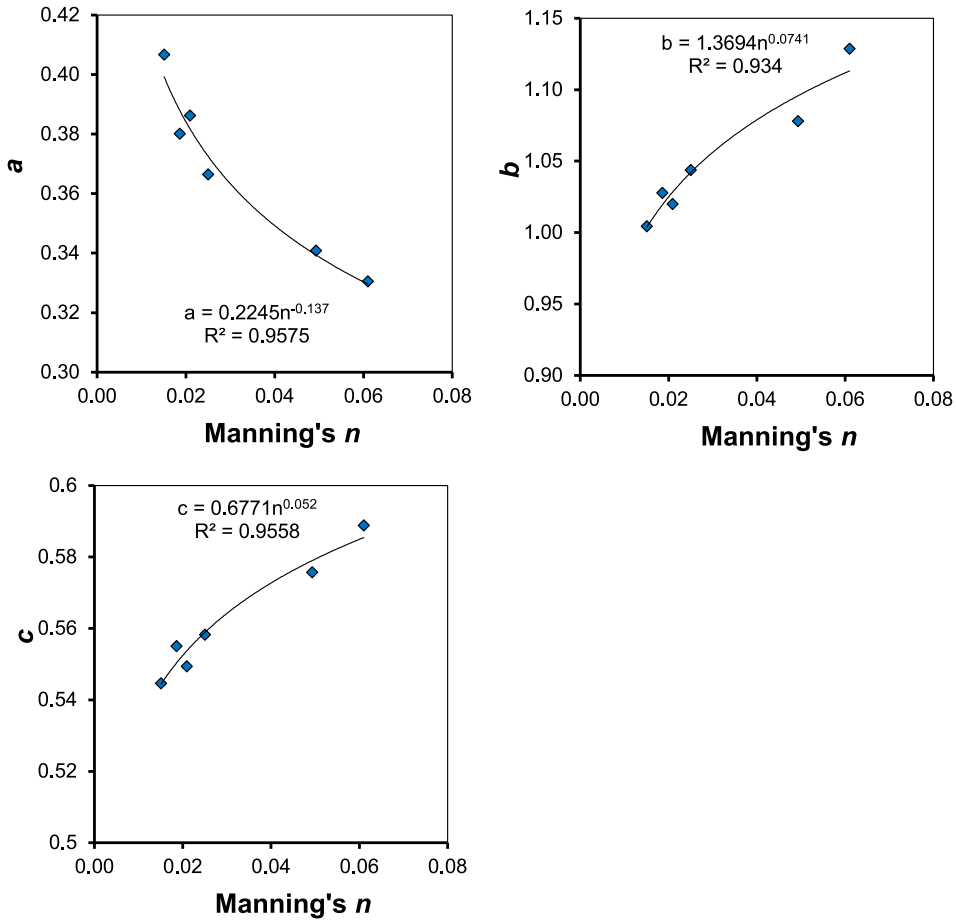

Fig. 11. Relationship between the values of the *a*, *b*, and *c* coefficients reported in Table 2 and the Manning's *n* values corresponding to the examined roughness.

reliability of the hypothesis to use *a* as the single coefficient affected by the roughness condition.

CRediT authorship contribution statement

Alessio Nicosia: Writing – review & editing, Writing – original draft, Methodology, Formal analysis, Data curation, Conceptualization. **Costanza Di Stefano:** Writing – review & editing, Writing – original draft, Investigation, Formal analysis, Data curation. **Vincenzo Palmeri:** Writing – review & editing, Writing – original draft, Formal analysis, Data curation, Conceptualization. **Maria Angela Serio:** Writing – review & editing, Writing – original draft, Formal analysis, Data curation, Conceptualization. **Vito Ferro:** Writing – review & editing, Writing – original draft, Supervision, Investigation, Formal analysis, Data curation, Conceptualization.

Declaration of competing interest

The authors declare that they have no known competing financial interests or personal relationships that could have appeared to influence the work reported in this paper.

Data availability

The data used in this paper are available at the following link: https://doi.org/10.6084/m9.figshare.17142440.v1

Acknowledgements

All authors set up the research, analyzed and interpreted the results and contributed to write the paper. This research did not receive any specific grant from funding agencies in the public, commercial, or not-for-profit sectors.

Appendix A

These similarity parameters are generated by using *y*, u_*, and μ as dimensional independent variables and combining the original dimensionless groups (Barenblatt, 1987):

$$\Pi_1 = \frac{y}{u_*}\frac{dv}{dy} \tag{1A}$$

$$\Pi_{2,3} = \frac{\Pi_2}{\Pi_3} = \frac{h}{y}\frac{y}{d} = \frac{h}{d} \tag{2A}$$

$$\Pi_4 = s \tag{3A}$$

$$\Pi_6 = \frac{u_* y}{\nu_k} \tag{4A}$$

$$\Pi_{5,2,6} = \Pi_5 \Pi_2 \Pi_6 = \frac{i}{u_*}\frac{h}{y}\frac{u_* y}{\nu_k} = \frac{ih}{\nu_k} = Re_i \tag{5A}$$

$$\Pi_{6,3,2} = \Pi_6 \Pi_3 \Pi_{2,3} = \frac{u_* y}{\nu_k}\frac{d}{y}\frac{h}{d} = \frac{u_* h}{\nu_k} \tag{6A}$$

$$\Pi_{7,2} = \sqrt{\frac{8}{f}}\ \frac{1}{\Pi_7^{1/2}\Pi_2^{1/2}} = \sqrt{\frac{8}{f}}\ \frac{u_*}{g^{1/2}y^{1/2}}\frac{y^{1/2}}{h^{1/2}} = \frac{\sqrt{\frac{8u_*^2}{f}}}{g^{1/2}h^{1/2}} = \frac{V}{\sqrt{gh}} = F \tag{7A}$$

The functional relationship (4) can be rewritten as:

$$\Pi_1 = \phi_2\left(\Pi_{2,3}, \Pi_4, \Pi_{5,2,6}, \Pi_6, \Pi_{6,3,2}, \Pi_{7,2}\right) \tag{8A}$$

where ϕ_2 is a functional symbol.

Introducing the expression of each dimensionless group into Eq. (8A), the following relationship is deduced:

$$\frac{y}{u_*}\frac{dv}{dy} = \phi_2\left(\frac{h}{d}, s, \frac{ih}{\nu_k}, \frac{u_* y}{\nu_k}, \frac{u_* h}{\nu_k}, F\right) \tag{9A}$$

Assuming the Incomplete Self-Similarity hypothesis in $u_* y/\nu_k$ (Barenblatt and Monin, 1979; Barenblatt and Prostokishin, 1993; Butera et al., 1993; Ferro and Pecoraro, 2000; Ferro, 2017), and integrating Eq. (9A) (Butera et al., 1993; Barenblatt and Prostokishin, 1993; Ferro and Pecoraro, 2000, Nicosia et al., 2020b) the following power velocity distribution is obtained:

$$\frac{v}{u_*} = \left[\frac{1}{\delta}\phi_3\left(\frac{u_* h}{\nu_k}, \frac{h}{d}, s, Re_i, F\right)\right]\left(\frac{u_* y}{\nu_k}\right)^{\delta} \tag{10A}$$

in which ϕ_3 is a functional symbol and δ is an exponent.

References

Abrahams, A.D., Parsons, A.J., Wainwright, J., 1994. Resistance to overland flow on semiarid grassland and shrubland hillslopes, Walnut Gulch, southern Arizona. J. Hydrol. 156 (1–4), 431–446.

Barenblatt, G.I., 1987. Dimensional Analysis. Gordon & Breach, Science Publishers Inc., Amsterdam.

Barenblatt, G.I., 1993. Scaling laws for fully developed turbulent shear flows, part 1, Basic hypothesis and analysis. J. Fluid Mech. 248, 513–520.

Barenblatt, G.I., Monin, A.S., 1979. Similarity laws for turbulent stratified flows. Arch. Ration. Mech. Anal. 70, 307–317.

Barenblatt, G.I., Prostokishin, V.M., 1993. Scaling laws for fully developed turbulent shear flows, part 2. Processing of experimental data. J. Fluid Mech. 248, 521–529.

Butera, L., Ridolfi, L., Sordo, S., 1993. On the hypothesis of self-similarity for the velocity distribution in turbulent flows. Excerpta 8, 63–94.

Castaing, B., Gagne, Y., Hopfinger, E.J., 1990. Velocity probability density functions of high Reynolds number turbulence. Physica D 46, 177–200.

Cen, Y., Zhang, K., Peng, Y., Rubinato, M., Liu, J., Ling, P., 2022. Experimental study on the effect of simulated grass and stem coverage on resistance coefficient of overland flow. Hydrol. Process. 36 (10), e14705.

Di Stefano, C., Ferro, V., Palmeri, V., Pampalone, V., 2017. Flow resistance equation for rills. Hydrol. Process. 31, 2793–2801.

Di Stefano, C., Nicosia, A., Palmeri, V., Pampalone, V., Ferro, V., 2021. Estimating flow resistance in steep slope rills. Hydrol. Process. 35, e14296.

Di Stefano, C., Nicosia, A., Palmeri, V., Pampalone, V., Ferro, V., 2022a. Rill flow velocity and resistance law: A review. Earth Sci. Rev. 231, 104092 https://doi.org/10.1016/j.earscirev.2022.104092.

Di Stefano, C., Nicosia, A., Palmeri, V., Pampalone, V., Ferro, V., 2022b. Rill flow resistance law under sediment transport. J. Soil. Sediment. 1–14.

Emmett, W.W., 1970. The hydraulics of overland flow on hillslopes: Dynamic and descriptive studies of hillslopes. Geol. Surv. Prof. Pap. A1–A67.

Ferro, V., 1997. Applying hypothesis of self-similarity for flow-resistance law of small-diameter plastic pipes. J. Irrigat. Drain. Eng. ASCE 123, 175–179.

Ferro, V., 2017. New flow resistance law for steep mountain streams based on velocity profile. J. Irrigat. Drain. Eng. ASCE 143 (04017024), 1–6. https://doi.org/10.1061/(ASCE)IR.1943-4774.0001208.

Ferro, V., 2018. Assessing flow resistance in gravel bed channels by dimensional analysis and self similarity. Catena 169, 119–127. https://doi.org/10.1016/j.catena.2018.05.034.

Ferro, V., 2019. Assessing flow resistance law in vegetated channels by dimensional analysis and self-similarity. Flow Meas. Instrum. 69 https://doi.org/10.1016/j.flowmeasinst.2019.101610.

Ferro, V., Nicosia, A., 2020. Comment on "Effects of different tillage practices on the hydraulic resistance of concentrated flow on the loess plateau in China" by J. Sun et al. Catena 193, 104629. https://doi.org/10.1016/j.catena.2020.104629.

Ferro, V., Pecoraro, R., 2000. Incomplete self-similarity and flow velocity in gravel bed channels. Water Resour. Res. 36, 2761–2770.

Ferro, V., Porto, P., 2018. Applying hypothesis of self-similarity for flow resistance law in Calabrian gravel bed rivers (Fiumare). J. Hydraul. Eng. ASCE 144, 1–11. https://doi.org/10.1061/(ASCE)HY.1943-7900.0001385.

Govers, G., 1992. Relationship between discharge, velocity and flow area for rills eroding loose, non-layered materials. Earth Surf. Proc. Land. 17, 515–528.

Hinsberger, R., Biehler, A., Yörük, A., 2022. Influence of water depth and slope on roughness-experiments and roughness approach for rain-on-grid modeling. Water 14 (24), 4017.

[dataset] Hinsberger, R., Biehler, A., Yörük, A., 2021. Data to a novel flow resistance approach for shallow water depth in overland flow simulations. figshare. Dataset. doi: 10.6084/m9.figshare.17142440.v1.

Katz, D.M., Watts, F.J., Burroughs, E.R., 1995. Effects of surface roughness and rainfall impact on overland flow. J. Hydraul. Eng. ASCE 121, 546–553.

Kowobari, T.S., Rice, C.E., Garton, J.E., 1972. Effect of roughness elements on hydraulic resistance for overland flow. Trans. ASAE 979–984.

Liu, C., Zhang, K., Wei, S., Wang, P., Cen, Y., Xia, J., 2023. Evaluation of the effects of grass and shrub cover on overland flow resistance and its attributes under simulated rainfall. J. Hydrol. 626, 130285.

Ma, L., Pan, C., Liu, J., 2022. Overland flow resistance and its components for slope surfaces covered with gravel and grass. Int. Soil Water Conserv. Res. 10 (2), 273–283.

Nearing, M.A., Polyakov, V.O., Nichols, M.H., Hernandez, M., Li, L., Zhao, Y., Armendariz, G., 2017. Slope–velocity equilibrium and evolution of surface roughness on a stony hillslope. Hydrol. Earth Syst. Sci. 21, 3221–3229.

Nicosia, A., Di Stefano, C., Pampalone, V., Palmeri, V., Ferro, V., Polyakov, V., Nearing, M.A., 2020a. Testing a theoretical resistance law for overland flow under simulated rainfall with different types of vegetation. Catena 189, 104482. https://doi.org/10.1016/j.catena.2020.104482.

Nicosia, A., Di Stefano, C., Palmeri, V., Pampalone, V., Ferro, V., 2020b. Flow resistance of overland flow on a smooth bed under simulated rainfall. Catena 187, 104351. https://doi.org/10.1016/j.catena.2019.104351.

Nicosia, A., Di Stefano, C., Pampalone, V., Palmeri, V., Ferro, V., Nearing, M.A., 2020c. Testing a theoretical resistance law for overland flow on a stony hillslope. Hydrol. Process. 1–9 https://doi.org/10.1002/hyp.13709.

Nicosia, A., Bischetti, G.B., Chiaradia, E., Gandolfi, C., Ferro, V., 2021. A full-scale study of Darcy-Weisbach friction factor for channels vegetated by riparian species. Hydrol. Process. 35 (3), e14009.

Nicosia, A., Ferro, V., 2023. Flow resistance due to shrubs and woody vegetation. Flow Measurement and Instrumentation 89, 102308.
Polyakov, V., Stone, J., Holifield Collins, C., Nearing, M.A., Paige, G., Buono, J., Gomez-Pond, R., 2018. Rainfall simulation experiments in the southwestern USA using the Walnut Gulch Rainfall Simulator. Earth Syst. Sci. Data 10, 19–26. https://doi.org/10.5194/essd-10-19-2018.
Shen, H.W., Li, R., 1973. Rainfall effect on sheet flow over smooth surface. J. Hydraul. Div. ASCE 99, 771–792.
Sun, J., Govers, G., Shi, M., Zhai, Y., Wu, F., 2020. Effects of different tillage practices on the hydraulic resistance of concentrated flow on the Loess Plateau in China. Catena 185, 104293.
Toy, T.J., Foster, G.R., Renard, K.G., 2002. Soil Erosion: Processes, Prediction, Measurement, and Control. John Wiley & Sons Inc, New York, USA.
Yoon, Y.N., Wenzel, H.G., 1971. Mechanics of sheet flow under simulated rainfall. J. Hydraul. Div. ASCE 97, 1367–1385.
Zhang, L., Zhang, S., Huang, H., 2024. Study on the resistance characteristics of layered vegetation to overland flow. Ecohydrology e2621.